Modeling and performance analysis of open-loop remotely operated vehicles ORCA

Tejaswini Panati, Sai Deepika Indraganti, Sakthivel Murugan Santhanam
Underwater Acoustic Research Laboratory, Department of Electronics and Communication Engineering, Sri Sivasubramaniya Nadar College of Engineering, Kalavakkam, Chennai, India

Article Info	**ABSTRACT**

ORCA is a low cost remotely operated vehicle which was indigenously developed for underwater inspection and survey. As the underwater environment is quite unpredictable, dynamic modeling and simulation of the remotely operated vehicle are essential to understand the behavior of the vehicle and accomplish stabilized navigation. This paper discusses a detailed approach to the mathematical modeling of ORCA based on Newtonian dynamics and simulating the position and velocity responses in Simulink. The open loop nonlinear model of the remotely operated vehicle was used to study the navigation challenges due to the various perturbations present underwater namely Coriolis and centripetal force, added mass, hydrodynamic damping force, and restoring forces. The six-thruster open loop ORCA model was subjected to various thrust inputs (25%, 50%, and 75%) to achieve six degrees of freedom (DoF) respectively and it was observed that there was significant instability in the other DOFs along with the principal direction of motion. Further, the authors will incorporate the various control systems in ORCA and analyze the stability in navigation induced due to each of them.

Corresponding Author:

Tejaswini Panati
Underwater Acoustic Research Laboratory, Department of Electronics and Communication Engineering,
Sri Sivasubramaniya Nadar College of Engineering, Kalavakkam, Chennai, 603110, India
Email: tejaswini17176@ece.ssn.edu.in

1. INTRODUCTION

The tethered underwater robots known as remotely operated vehicles (ROV) are frequently employed for underwater survey and inspection. They are unmanned, highly maneuverable underwater vehicles that can be used to explore ocean depths while being operated remotely by a user at the water's surface. They are extensively utilized for both scientific reasons like ocean exploration and industrial ones like internal and external inspections of underwater pipelines and the structural assessment of offshore structures. Recently, a number of ROV applications for ocean research have been reported [1]–[4]. Based on the application, they range in their size from a micro or mini ROV which is used to reach areas at shallow depths to a work class ROV which is used for ocean floor exploration and inspection at unreachable depths. They serve to be greatly beneficial due to quick deployment, minimal maintenance, the ability to fit into confined areas, extended dive times, and video recording capabilities. Aquaculture, search and rescue, underwater intervention, repair, and maintenance work in offshore businesses, such as the oil and gas industry, marine structures, marine sciences, naval defense, marine renewable energy, and research reasons are just a few of the uses for these underwater ROVs [5]–[11]. ROVs enables users to capture photos and videos to inspect and monitor ports, harbors, and vessels, locate underwater targets, and explore the depths of our oceans. ROVs are equipped with manipulators and multiple sensors to conduct survey and inspection activities. Sensors like altimeters, pressure sensors, inclinometers, and magnetic and gyrocompass are also

used to help ROVs understand their environment [12]. ROVs frequently have cameras for surveillance and streaming video. The design and implementation of Aqua bot is discussed [13], an ROV constructed with the goal of addressing issues with real-time video streaming and other development methods. Numerous localization and navigation techniques, including dead reckoning and inertial navigation systems, are in use. These include acoustic navigation, geophysical navigation, fusion of long baseline (LBL), and doppler-based techniques [14], [15].

In today's world, computer-aided designs of engineering systems as models are performed. They are the next step after designing. They come in handy in documentation and quality assurance. These models can hence be used in various ways by firms and people who install, commission, and operate subsea installations and equipment. Simulation software has always been a boon to the product development process because they give an opportunity to rehearse certain conditions of operation to test for worst-case and best-case scenarios. Workflow analyses, contingency plans, and training scenarios for the pilots and technicians who will perform the tasks can be thus provided for ease of development. Mathematical models have been developed to design the dynamics of an ROV and other underwater vehicles. These models have been successfully adapted by many ROVs for performing various activities [16]–[18]. Since an underwater channel is highly dynamic, it is necessary to have an effective control system for stabilized movement [19]–[21]. Different control systems with varying levels of efficiency can be created for ROVs [22], [23].

This paper addresses broadly the development of a mathematical model of the ORCA ROV and analyze the position and velocity responses obtained from its simulation. The first section briefs on the design and development of ORCA and throws light on its capabilities to conduct an efficient inspection. The second section presents detailed mathematical modeling and the necessary design parameters of ORCA required to simulate the nonlinear open loop model and study its response. It further projects the Simulink model of the ORCA ROV and briefly discusses the various subsystems. Finally, the last section presents the performance evaluation of nonlinear open-loop ORCA when subjected to different input thrusts for the desired time to study the instability in the position and velocity responses for the six degrees of freedom namely surge, sway, heave, roll, yaw, and pitch.

2. SYSTEM DESIGN

In this section, the basic design of the ORCA ROV is elaborated. ORCA ROV, as shown in Figures 1 and 2, is a 500×350×210 mm³ vehicle weighing 10.247 kgs which is equipped with sensors like temperature, and pressure, an IMU, and a camera for use in the primary underwater inspection and survey application until a depth of 300 m. It was indigenously developed by the authors and team and the novel feature of ORCA is shown in Table 1.
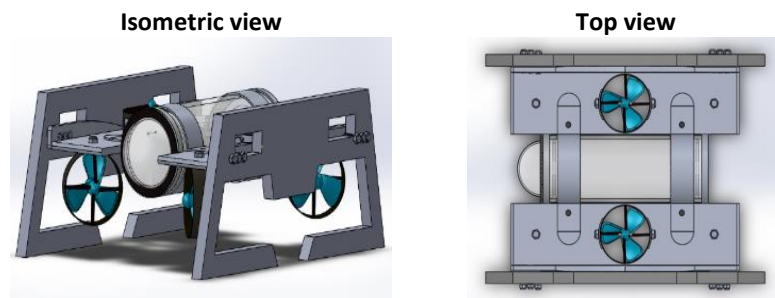

Figure 1. CAD design of ORCA ROV

Figure 2. Fabricated ORCA ROV

High-density polyethylene (HDPE) was used to make the six-thruster ROV. It has two body-mounted sealed acrylic enclosures for the battery and electronics, respectively. The embedded electronic system integrated with sensors as shown in Figure 3 is responsible for achieving the desired movement of the vehicle as per the joystick command. The robust navigation is achieved due to the presence of the attitude and heading reference system, a sensor fusion algorithm that obtains the IMU raw data to compute the current position and attitude of the vehicle. The whole system is powered using the 14.8 V, 18 Ah Li-ion battery. The versatility of ORCA has increased due to the freedom in placing the T200 thrusters at two different orientations. It has four thrusters mounted at 45 degrees to the x and y axes for active control of surge, sway, yaw, and two dedicated thrusters to achieve heave or roll, thereby enabling active control of 5 degrees of freedom (DoF) and passive pitch control. An effective thrust vectorization algorithm was developed to achieve best-in-class maneuverability.

Table 1. Novel features of ORCA

S. No.	Unique Features of ORCA	Remarks
1	Flexible thruster mounting. The four horizontal thrusters can be manually swiveled and mounted at 30, 45 or 60 w.r.t the heading axis.	Gives rise to different possible vectored thrust configurations. This helps us to customize ORCA as per the underwater environment to tackle the varying currents.
2	Open-source software platform (MOOS-IVP) Exclusively customized application was developed for remote operation of the vehicle using this platform. Easy integration of various sensors.	This gives rise to use integrate many sensors to the vehicle in ease as the development does not involve any dedicated hardware.
3	Effective thrust vectorization algorithm Algorithm developed on the controller end to achieve navigation in 6-DoF.	Easy and best in class maneuverability with active control in 5 degrees of freedom with passive pitch control.
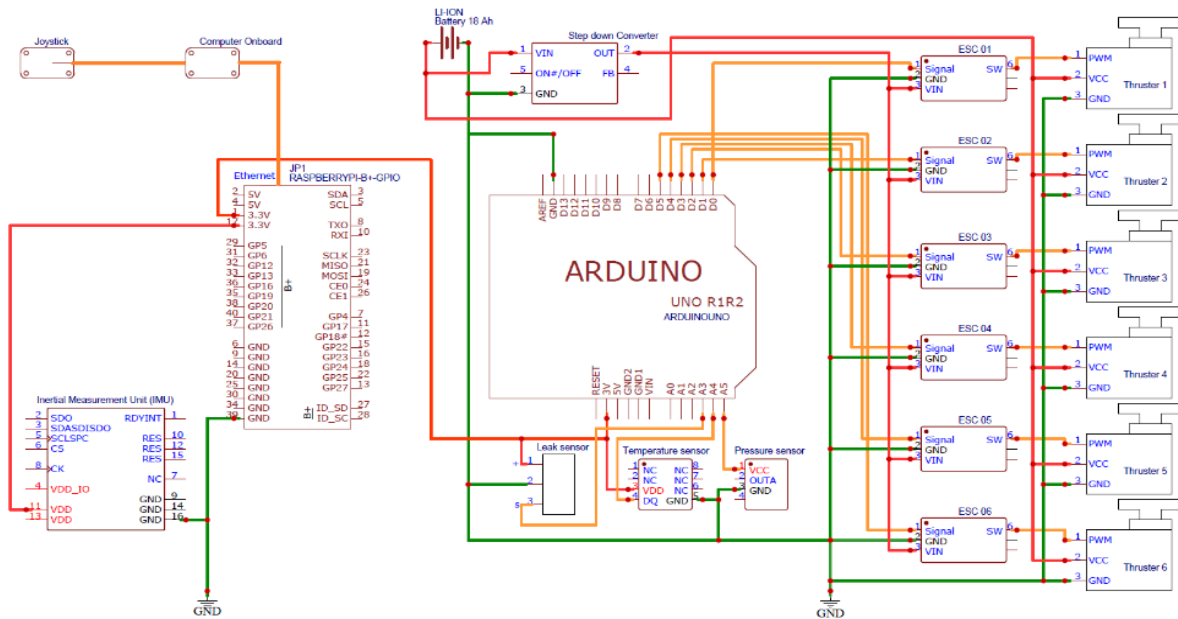
Figure 3. Electronic circuitry scheme in ORCA

3. OPEN LOOP MODELING OF ORCA

To understand the motion of ORCA in underwater environments subjected to various perturbations it is required to mathematically model the ROV and simulate the position responses. The dynamic model for ORCA is derived based on the Newtonian approach as adopted from [21]. The two frames of reference, the inertial frame or the earth-fixed frame, and the local body fixed frame with its origin coinciding with the vehicle's center of gravity are considered to define the movement of ORCA ROV in three-dimensional space. The assumptions considered to model ORCA ROV involves that i) ROV is a rigid body fully submerged in water; ii) disturbance due to a wave is neglected as the ROV is fully submerged in water; and iii) the earth-fixed frame of reference is inertial; and ROV is assumed to be moving slowly to carry out the inspection.

The 6 DoF nonlinear equation of motion of ROV in body fixed frame required to mathematically model ORCA is given by (1).

$$M\dot{v} + C(v)v + D(v)v + G_f(\eta) = \tau \tag{1}$$

where **M** is the mass inertia matrix which is **the** sum of the rigid body inertia mass and added fluid inertia mass matrix, $M = M_{RB} + M_A \in R^{6\times6}$; **C(v)** is the Coriolis and centripetal force matrix which contains the rigid body and added mass terms respectively, $C(v) = C_{RB}(v) + C_A(v) \in R^{6\times6}$; $D(v) \in R^{6\times6}$ is the damping matrix due to the surrounding fluid; $G_f(\eta) \in R^{6\times1}$ is used to describe the gravitational and buoyancy force on the ROV; $\tau \in R^{6\times1}$ is the total force or thrust vector in a given degree of freedom; $v = [\ u\ v\ w\ p\ q\ r\ ]^T$ is the body-fixed velocity vector and $\eta = [\eta_1\ \eta_2]^T$ is the earth-fixed position and orientation vector where $\eta_1 = [x\ y\ z\ ]^T$ is the position vector and $\eta_2 = [\varphi\ \theta\ \psi\ ]^T$ is the orientation vector of Euler angles as per Table 2.

Table 2. Notations used for ROV

DoF	Motion Description	Forces and moments	Linear and angular velocity (in body-fixed frame)	Positions and Orientations (in earth-fixed frame)
1	Surge (Motion in the x-direction)	X	u	x
2	Sway (Motion in the y-direction)	Y	v	y
3	Heave (Motion in the z-direction)	Z	w	z
4	Roll (Rotation about x-axis)	K	p	φ
5	Pitch (Rotation about y-axis)	M	q	θ
6	Yaw (Rotation about z-axis)	N	r	ψ

Hence, it is evident from (1) that the three external forces, the damping force, the Coriolis force, and the gravitational and buoyancy restoring force acting on the ROV influence its navigation in an underwater environment. The rigid body mass inertia matrix represents the mass of the ROV and the spread of the mass in different directions in terms of the moment of inertia, which is given by

$$M_{RB} = \begin{bmatrix} m & 0 & 0 & 0 & mz_G & -my_G \\ 0 & m & 0 & -mz_G & 0 & mx_G \\ 0 & 0 & m & my_G & -mx_G & 0 \\ 0 & -mz_G & my_G & I_x & -I_{xy} & -I_{xz} \\ mz_G & 0 & -mx_G & -I_{yx} & I_y & -I_{yz} \\ -my_G & mx_G & 0 & I_{zx} & -I_{zy} & I_z \end{bmatrix}$$

where **m** represents the mass of the ROV, $r_G = [x_G\ y_G\ z_G]^T$ is the center of gravity, and $I = \begin{bmatrix} I_x & -I_{xy} & -I_{xz} \\ -I_{yx} & I_y & -I_{yz} \\ I_{zx} & -I_{zy} & I_z \end{bmatrix}$ represents the rigid body ROV's the inertia matrix where I_x, I_y and I_z are the moments of inertia about X,Y, and Z axes and the cross products of inertia $I_{xy} = I_{yx}$, $I_{xz} = I_{zx}$, and $I_{yz} = I_{zy}$. ORCA has its center of gravity at $r_G = [x_G\ y_G\ z_G]^T = [0\ 0\ 0]^T$ and an inertia matrix of

$$I = \begin{bmatrix} 0.16419 & -0.01493 & 0.00113 \\ -0.01496 & 0.34512 & -0.00063 \\ 0.00113 & -0.00063 & 0.24282 \end{bmatrix}$$

Therefore, the rigid body mass matrix of ORCA is

$$M_{RB} = \begin{bmatrix} 10.247 & 0 & 0 & 0 & 0 & 0 \\ 0 & 10.247 & 0 & 0 & 0 & 0 \\ 0 & 0 & 0 & 0 & 0 & 0 \\ 0 & 0 & 0 & 0.16419 & -0.01493 & 0.00113 \\ 0 & 0 & 0 & -0.01493 & 0.34512 & -0.00063 \\ 0 & 0 & 0 & 0.00113 & -0.00063 & 0.24282 \end{bmatrix}$$

The inertial force known as the Coriolis force acts on an object moving within a frame of reference that rotates with regard to another object. The Coriolis and centripetal forces on ROV are given by matrix as per the Newtonian dynamics:

$$C_{RB} = \begin{bmatrix} m\ [v_2\ x\ v_1\ +\ v_2\ x\ (v_2\ x\ r_G)] & m\ [v_2\ x\ v_1\ +\ v_2\ x\ (v_2\ x\ r_G)\ ] \\ v_2\ x\ (\ Iv_2)\ +\ mr_G\ x\ (v_2\ x\ v_1) & v_2\ x\ (\ Iv_2)\ +\ mr_G\ x\ (v_2\ x\ v_1) \end{bmatrix}$$

where m is the mass of ROV, $\mathbf{v_1} = [\mathbf{u\ v\ w}]^T$ and $\mathbf{v_2} = [\mathbf{p\ q\ r}]^T$ are the velocity vectors, $\mathbf{r_G}$ is the center of gravity of the ROV and $\mathbf{I}$ is the moment of inertia of the vehicle. The motion of the fluid around the vehicle due to the motion of the ROV causes a hydrodynamic negating force which will retard the motion of the ROV. The added mass matrix is given by:

$$M_A = \begin{bmatrix} X_{\dot{u}} & 0 & 0 & 0 & 0 & 0 \\ 0 & Y_{\dot{v}} & 0 & 0 & 0 & 0 \\ 0 & 0 & Z_{\dot{w}} & 0 & 0 & 0 \\ 0 & 0 & 0 & K_{\dot{p}} & 0 & 0 \\ 0 & 0 & 0 & 0 & M_{\dot{q}} & 0 \\ 0 & 0 & 0 & 0 & 0 & N_{\dot{r}} \end{bmatrix}$$

where $\mathbf{X_{\dot{u}}, Y_{\dot{v}}, Z_{\dot{w}}, K_{\dot{p}}, M_{\dot{q}}, and\ N_{\dot{r}}}$ are the hydrodynamic derivatives in the respective DoFs. The added mass matrix of ORCA is given by:

$$M_A = -\text{diag}\{2.98509, 7.30064, 17.23463, 0.38282, 1.87219, 0.719066\}$$

The corresponding Coriolis and centripetal added mass matrix $\mathbf{C_A(v)}$ are given by:

$$C_A = \begin{bmatrix} 0 & 0 & 0 & 0 & -Z_{\dot{w}}w & Y_{\dot{v}}v \\ 0 & 0 & 0 & Z_{\dot{w}}w & 0 & -X_{\dot{u}}u \\ 0 & 0 & 0 & -Y_{\dot{v}}v & X_{\dot{u}}u & 0 \\ 0 & -Z_{\dot{w}}w & Y_{\dot{v}}v & 0 & -N_{\dot{r}}r & M_{\dot{q}}q \\ Z_{\dot{w}}w & 0 & -X_{\dot{u}}u & N_{\dot{r}}r & 0 & -K_{\dot{p}}p \\ -Y_{\dot{v}}v & X_{\dot{u}}u & 0 & -M_{\dot{q}}q & K_{\dot{p}}p & 0 \end{bmatrix}$$

$$= \begin{bmatrix} 0 & 0 & 0 & 0 & -17.23463w & 7.30064v \\ 0 & 0 & 0 & 17.23463w & 0 & -2.98509u \\ 0 & 0 & 0 & -7.30064v & 2.98509u & 0 \\ 0 & -17.23463w & 7.30064v & 0 & -0.719006r & 1.87219r \\ 17.23463w & 0 & -2.98509u & 0.719006r & 0 & -0.38282p \\ -7.30064v & -2.98509u & 0 & -1.87219r & 0.38282p & 0 \end{bmatrix}$$

Hydrodynamic damping appears as the sum of the linear damping caused due to skin friction and quadratic damping due to vortex shedding. Hence, $D(v) = D_L + D_Q$, where

$$D_L = -\text{diag}\{X_u, Y_v, Z_w, K_p, M_q, N_r\}$$

$$D_Q = -\text{diag}\{X_{u|u|}, Y_{v|v|}, Z_{w|w|}, K_{p|p|}, M_{q|q|}, N_{r|r|}\}$$

represents the linear and quadratic damping coefficients. Calculating the respective drag coefficients for ORCA in 6-DoF, we obtain

$$D_L = -\text{diag}\{0.1682, 0.3727, 2.7871, 0, 0, 0\}$$

$$D_Q = -\text{diag}\{11.612, 46.197, 86.647, 0, 0, 0.3168\}$$

The restoring gravitational and buoyancy force vector acting on the ROV is given by

$$Gf(\eta) = \begin{bmatrix} (W - B)\sin\theta \\ -(W - B)\cos\theta\sin\phi \\ -(W - B)\cos\theta\cos\phi \\ -(y_G W - y_B B)\cos\theta\cos\phi + (z_G W - z_B B)\cos\theta\sin\phi \\ (z_G W - z_B B)\sin\theta + (x_G W - x_B B)\cos\theta\cos\phi \\ -(x_G W - x_B B)\cos\theta\sin\phi - (y_G W - y_B B)\sin\theta \end{bmatrix}$$

where $\mathbf{W}$ is the weight of the ROV, $\mathbf{B}$ represents the ROV buoyancy, and $[\phi\ \theta\ \psi]$ represents the Euler angles representing the orientation of the ROV. ORCA is designed to be positively buoyant with center of

Buoyancy, $\mathbf{r_B} = [\mathbf{x_B} \, \mathbf{y_B} \, \mathbf{z_B}]^T = [\ 0 \ 0 \ -0.0082]^T$. The weight and buoyancy of ORCA are found to be 100.52307 N. Hence the buoyancy and gravitational force matrix are

$$Gf\,(\eta) = \begin{bmatrix} 0 \\ 0 \\ 0 \\ 0.8242 \cos\theta \sin\phi \\ 0.8242 \sin\theta \\ 0 \end{bmatrix}$$

The input thrust generated by each of the six thrusters, $\mathbf{u} = [\mathbf{u_1} \, \mathbf{u_2} \, \mathbf{u_3} \, \mathbf{u_4} \, \mathbf{u_5} \, \mathbf{u_6}]^T$ is related to the force and moment vector generated in the 6-DoF, $\boldsymbol{\tau} = [\boldsymbol{\tau_x} \, \boldsymbol{\tau_y} \, \boldsymbol{\tau_z} \, \boldsymbol{\tau_\phi} \, \boldsymbol{\tau_\theta} \, \boldsymbol{\tau_\psi}]^T$, as

$$\tau = Tu \tag{2}$$

where **T** is the thrust configuration matrix which represents the position of each thruster from the center of gravity (COG) of the vehicle. Four of the six thrusters of ORCA are mounted at a 45° to the x and y-axes about the z axis, and the other two thrusters are mounted with its axis parallel to the z-axis. The thrust vectorization of ORCA is shown in Figure 4. The force and moment vector generated in 6-DoF is given by (3) to (8).

$$u_1 \sin\alpha + u_2 \sin\alpha + u_4 \sin\alpha + u_5 \sin\alpha = \tau_x \tag{3}$$

$$u_1 \cos\alpha - u_2 \cos\alpha - u_4 \cos\alpha + u_5 \cos\alpha = \tau_y \tag{4}$$

$$u_3 + u_4 = \tau_z \tag{5}$$

$$-yu_3 + yu_4 = \tau_\phi \tag{6}$$

$$u_1 z \sin\alpha + u_2 z \sin\alpha + u_3 z \sin\alpha + u_4 z \sin\alpha = \tau_\theta \tag{7}$$

$$u_1 x \cos\alpha - u_2 x \cos\alpha + u_3 x \cos\alpha - u_4 x \cos\alpha = \tau_\psi \tag{8}$$
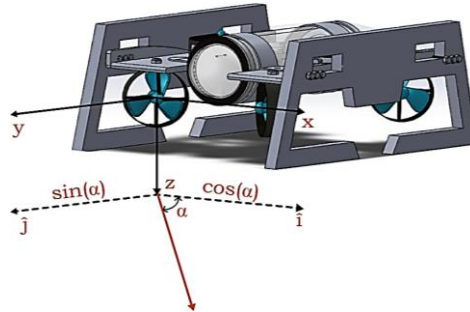
Figure 4. Thrust vectorization of ORCA

Hence, the thrust configuration matrix for ORCA is given by

$$T = \begin{bmatrix} \sin\alpha & \sin\alpha & 0 & 0 & \sin\alpha & \sin\alpha \\ \cos\alpha & -\cos\alpha & 0 & 0 & -\cos\alpha & \cos\alpha \\ 0 & 0 & 1 & 1 & 0 & 0 \\ 0 & 0 & -x & x & 0 & 0 \\ z\sin\alpha & z\sin\alpha & 0 & 0 & z\sin\alpha & z\sin\alpha \\ y\cos\alpha & -y\cos\alpha & 0 & 0 & y\cos\alpha & -y\cos\alpha \end{bmatrix}$$

where **α** is angle at which the thruster is mounted (30°, 45°, or 60°), **x** is distance of the thruster from the COG along x axis, **y** is distance of the thruster from the COG along y axis and **z** is the distance from the COG along z axis. By substituting:

$$
\begin{bmatrix} \tau_x \\ \tau_y \\ \tau_z \\ \tau_\phi \\ \tau_\theta \\ \tau_\psi \end{bmatrix} = \begin{bmatrix} 0.7071 & 0.7071 & 0 & 0 & 0.7071 & 0.7071 \\ 0.7071 & -0.7071 & 0 & 0 & -0.7071 & 0.7071 \\ 0 & 0 & 1 & 1 & 0 & 0 \\ 0 & 0 & -0.110 & 0.110 & 0 & 0 \\ 0.0176 & 0.0176 & 0 & 0 & 0.0176 & 0.0176 \\ 0.1237 & -0.1237 & 0 & 0 & 0.1237 & -0.1237 \end{bmatrix} \begin{bmatrix} u_1 \\ u_2 \\ u_3 \\ u_4 \\ u_5 \\ u_6 \end{bmatrix}
$$

the dynamics in the body-fixed frame are transformed to earth-fixed frame using Euler's angles. The kinematic equation representing the Euler transformation is (9),

$$\dot{\eta} = J(\eta)v \tag{9}$$

where the Euler transformation matrix $J(\eta)$ is taken from a successive rotation of the Euler's angles $\eta_2 = [\varphi \theta \psi]^T$ about Z, Y, and X axes.

$$
\begin{bmatrix} \eta \\ \dot{\eta} \end{bmatrix} = \begin{bmatrix} I & 0 \\ 0 & J(\eta_2) \end{bmatrix} \begin{bmatrix} \eta \\ v \end{bmatrix}
$$

$$
J(\eta 2) = \begin{bmatrix} J_1(\eta 2) & 0 \\ 0 & J_2(\eta 2) \end{bmatrix}
$$

where

$$
J_1(\eta 2) = \begin{bmatrix} c(\psi)c(\theta) & -s(\psi)c(\phi) + c(\psi)s(\theta)s(\phi) & s(\psi)s(\phi) + c(\psi)c(\phi)s(\theta) \\ s(\psi)c(\theta) & c(\psi)c(\phi) + s(\phi)s(\theta)s(\psi) & -c(\psi)s(\phi) + s(\theta)s(\psi)c(\theta) \\ -s(\theta) & c(\theta)s(\phi) & c(\theta)c(\phi) \end{bmatrix}
$$

$$
J_2(\eta 2) = \begin{bmatrix} 1 & s(\phi)t(\theta) & c(\phi)t(\theta) \\ 0 & c(\phi) & -s(\phi) \\ 0 & \dfrac{s(\phi)}{c(\theta)} & \dfrac{c(\phi)}{c(\theta)} \end{bmatrix}
$$

where s=sin(.), c=cos(.), and t=tan(.). Therefore, this transformation converts the velocity vector in the body-fixed frame to the position and orientation vector in earth fixed inertial frame. Having the model as the basis, the simulation of the ORCA ROV was performed in Simulink to analyze the position and velocity response for the 6-DoF and understand the navigation challenges in the present open loop system.

As shown in Figure 5, the nonlinear open loop model consists of five subsystems namely, thrust configuration block, inertial and added a mass block, Coriolis and centripetal block, gravitational force block, and Euler transformation block. The nonlinearity in the model is due to the external forces impacting its navigation in the underwater environment. This model with the subsystems realizes (10).

$$\dot{v} = M^{-1}\{\tau - [C(v)v + D(v)v + G_f(\eta)]\} \tag{10}$$

The acceleration vector obtained is integrated to form the body-frame velocity vector and then further transformed into the inertial frame position and orientation vector. The position and velocity responses obtained for a given input thrust and desired simulation time are analyzed in the following section to understand the navigation challenges in ORCA ROV.

4.   PERFORMANCE ANALYSIS OF NONLINEAR OPEN LOOP POSITION AND VELOCITY RESPONSES FOR ORCA

The performance analysis involved a lot of intensive testing of the model of ROV-ORCA, by varying the input parameters and observing the outputs. ORCA is a six-thruster model with thrusters 1, 2, 5, and 6 and thrusters 3 and 4 as shown in Figure 5 for movement in the horizontal plane and the vertical plane, respectively. The authors have considered a shallow water channel for modeling which has a density of 998.2 kg/m^3, viscosity of 0.001003 N.s/m^2, and pressure of 1.02 bar at 25 °C. Thrust for each of the 6 thrusters is given in the form of input and the navigation behavior of ORCA is observed at the output by means of velocity and position response graphs. ORCA is equipped with T200 thrusters which can produce a maximum of 4.53 KgF in a clockwise direction and 3.5 KgF in an anticlockwise direction. Varying input

thrust was provided, and the responses were generated with input to be 25% of the maximum thrust advisable for the thrusters, then at 50% thrust, and then at 75% thrust. At each of these input cases, a time variation from 10 seconds to 300 seconds was given, and the responses were recorded. Shown here are responses to an input of 50% thrust (2.265 KgF).
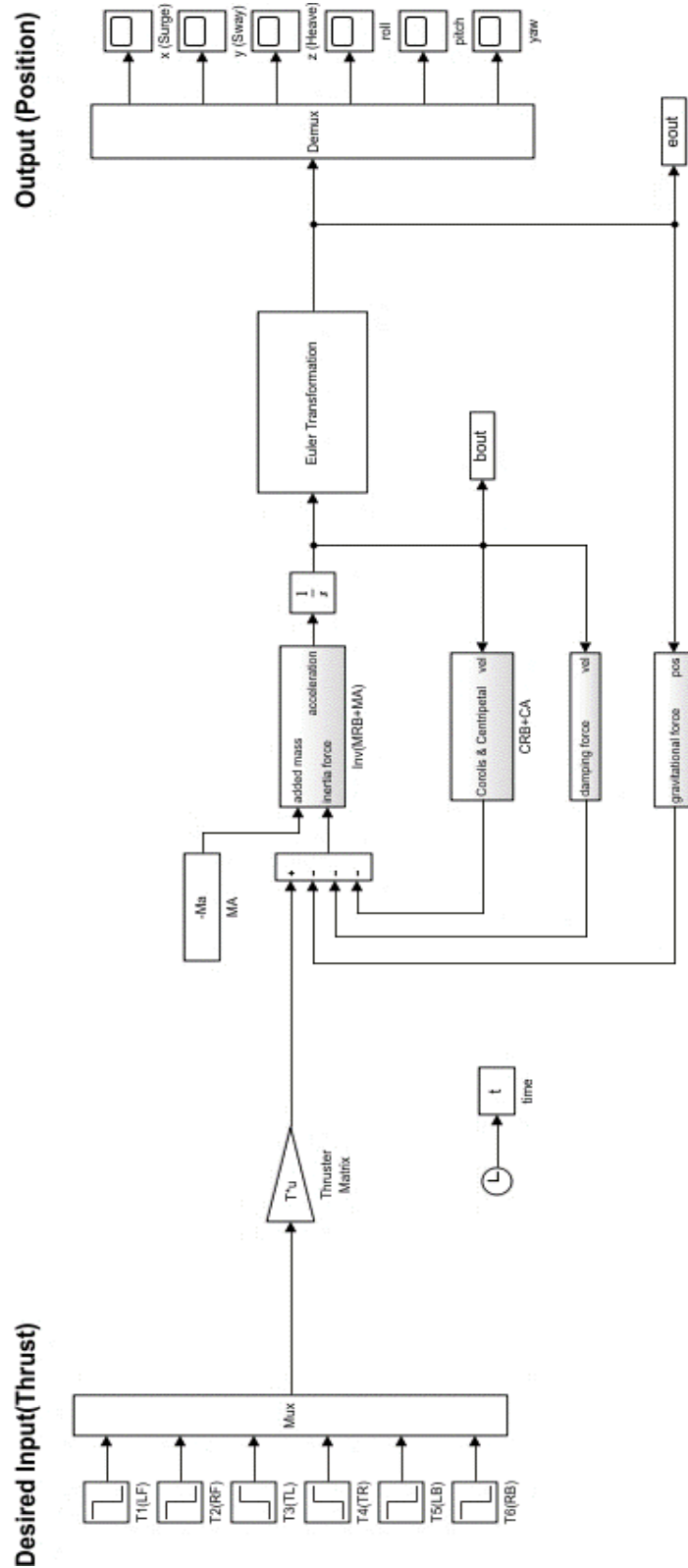

Figure 5. Nonlinear open loop ROV model for simulation

Figure 6 represents the velocity and position response of ORCA when commanded to surge forward. To achieve this response, the thrusters T1, T2, T5, and T6 in Figure 5 were provided with +2.265 KgF thrust for 300 seconds. As observed in Figure 6, ORCA actively surged with a velocity of 0.6-0.8 m/sec to cover a distance of 200 m in 5 minutes. Surge being the principal direction of navigation in this case there is a predominant increase in the distance moved by ORCA in the x direction. While it can be observed that in the other linear directions like the sway and heave there is still some amount of disturbance due to the action of the damping and Coriolis forces due to which the ROV ends up at 1m to the right and 0.4 m deep after 300 seconds. While the disturbance in the form of roll and pitch is minimal it is observed that the system yaws to almost 4.5 degrees. Hence, there is some instability induced in other degrees of freedom along with the movement of the ROV in the x direction.

(a)

(b)
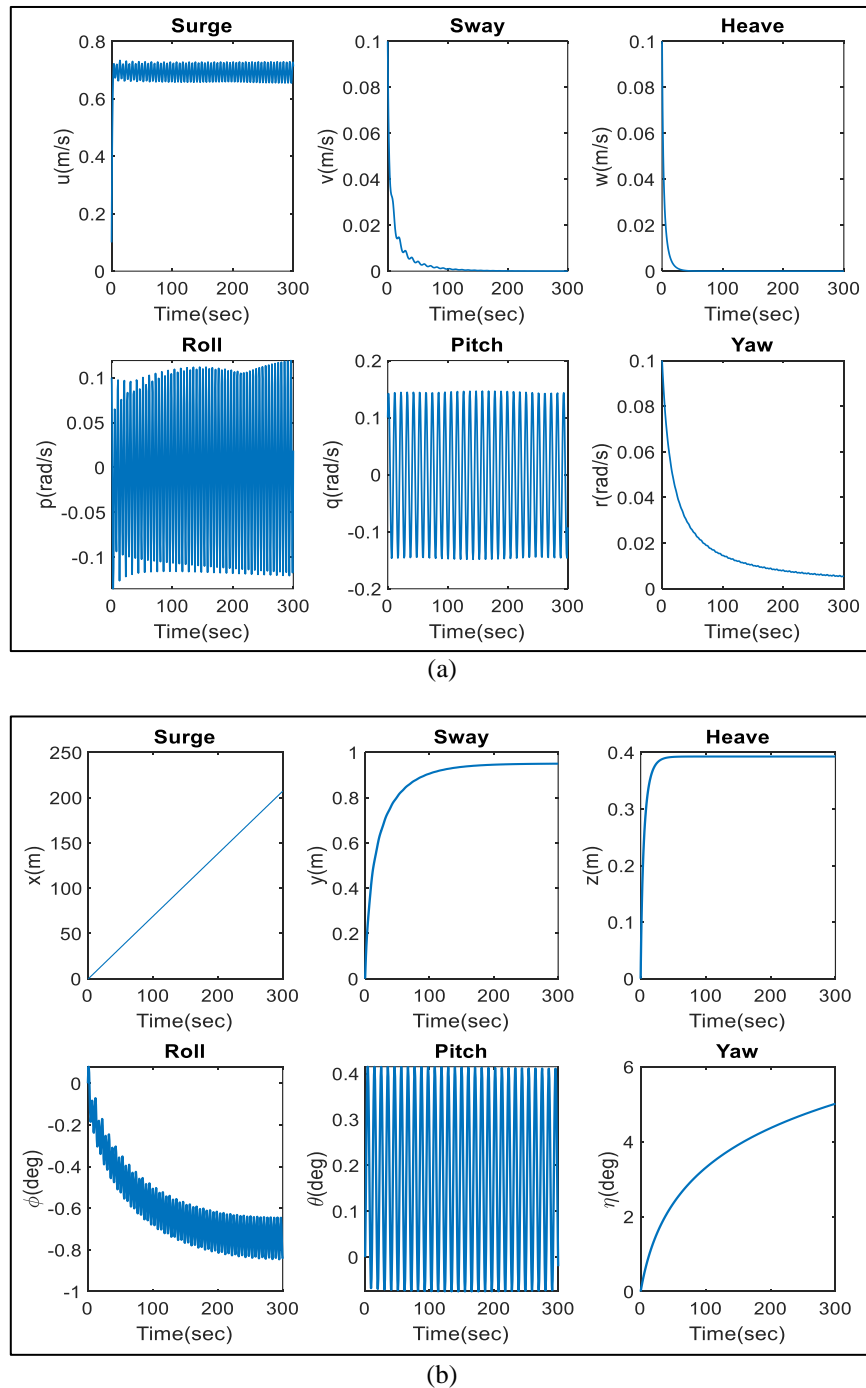
Figure 6. Performance of ORCA in surge direction: (a) velocity and (b) position response

Figure 7 represents the velocity and position response of ORCA when commanded to sway right. To achieve this response, as per the thrust vectorization, the thrusters T1 and T6 in Figure 5 were provided with +2.265 kgf thrust, and T2 and T5 were provided with -2.265 kgf thrust for 300 seconds. As observed in Figure 7, ORCA sways right with a velocity of 0.3-0.4 m/sec to cover a distance of 100 m right in 5 minutes. Along with swaying right, it is observed that there is still some amount of disturbance due to the action of the damping and Coriolis forces due to which the ROV ends up at 2.2 m forward and 0.4 m deep after 300 seconds. In comparison to the surge case, the roll induced in the vehicle has been reduced while the pitch and yaw effects remain the same.
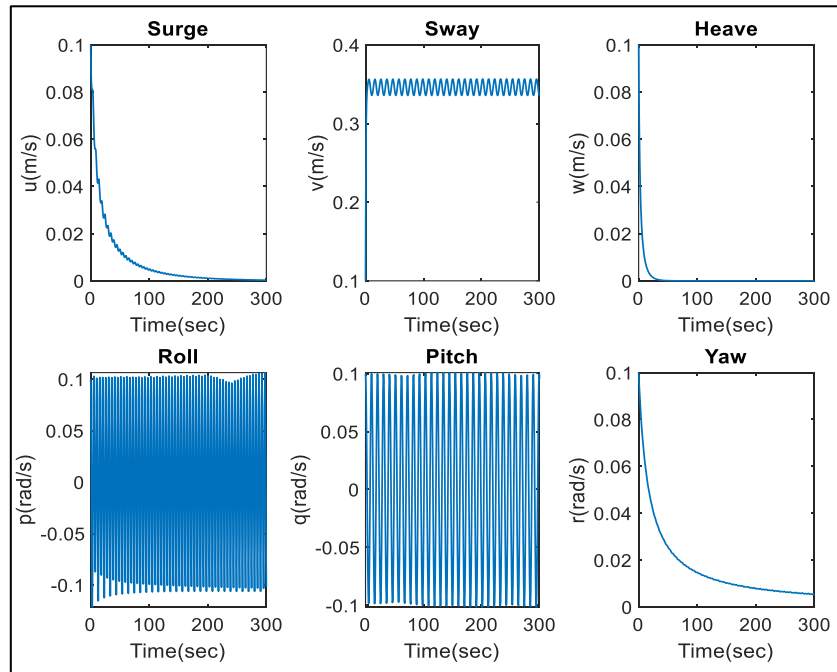
(a)
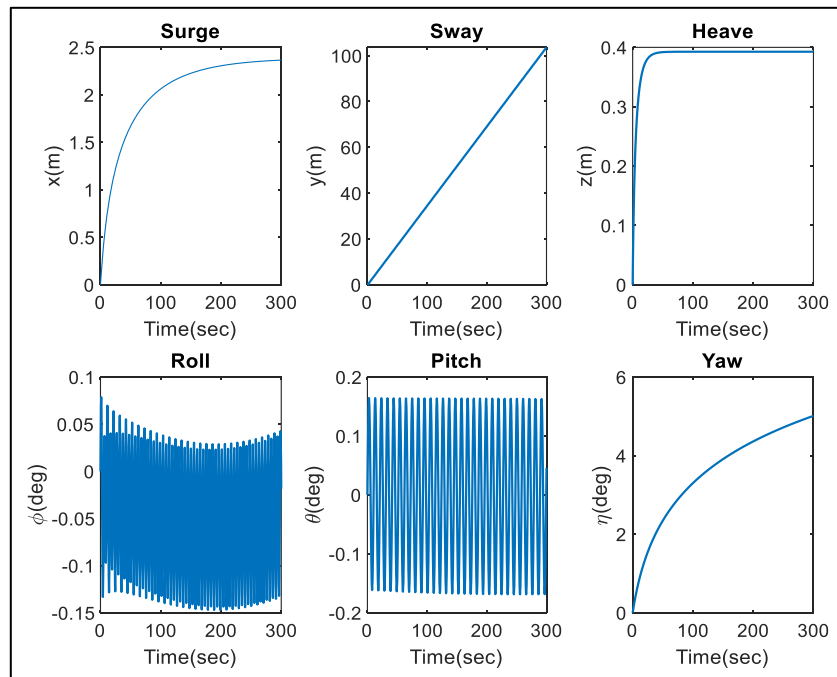
(b)

Figure 7. Performance of ORCA in sway direction: (a) velocity and (b) position response

Similarly, for each degree of freedom (heave motion in Figure 8, yaw motions in Figure 9, and roll motions Figure 10), a careful analysis was performed and keen observations on other non-principal directions were made. Hence, an overall inference from the performance analysis is the thrust input given to each thruster increases for a given DoF, the distance moved in the principal direction for the same time interval also increases. It is observed that with time, the error gets aggregated. Along with the negating forces (damping, Coriolis, and restoring force) acting on the ROV, it reflects as a disturbance in other directions too. This gave the authors a clear picture of instability in certain degrees of freedom. These directions are recommended to use a controller for smooth navigation as it helps us in the reduction of errors. Hence, the control system plays a vital role in nullifying unnecessary deviations and helps us achieve stabilized navigation.
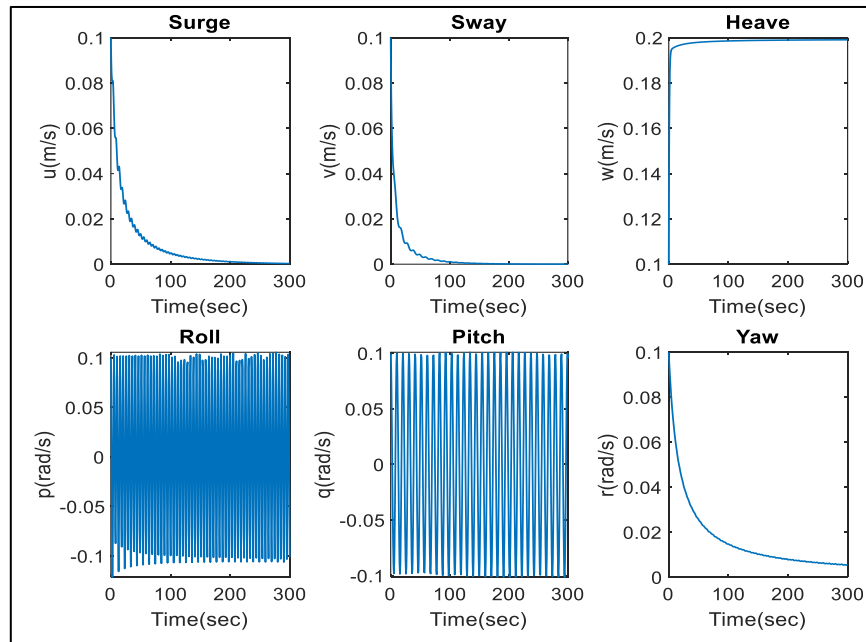
(a)
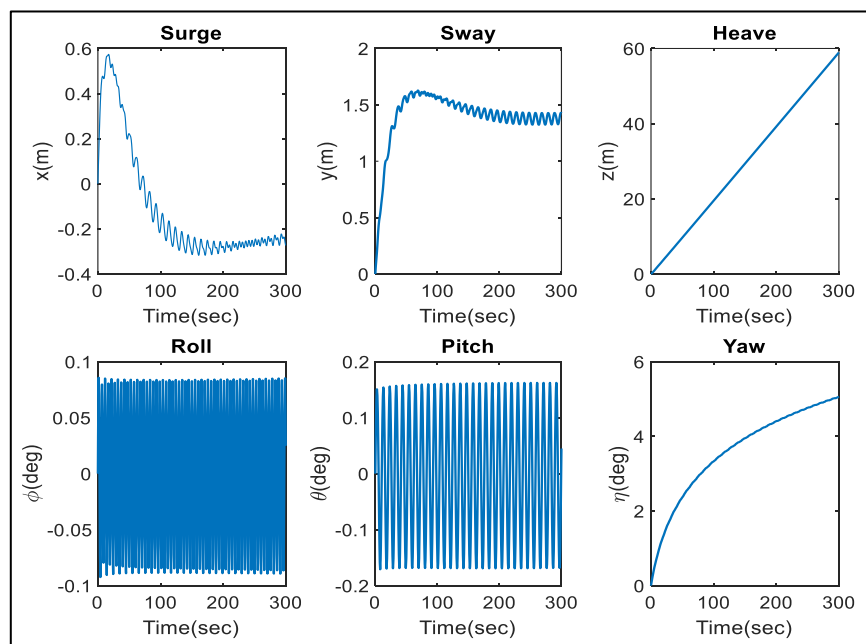
(b)

Figure 8. Performance of ORCA in heave direction: (a) velocity and (b) position response
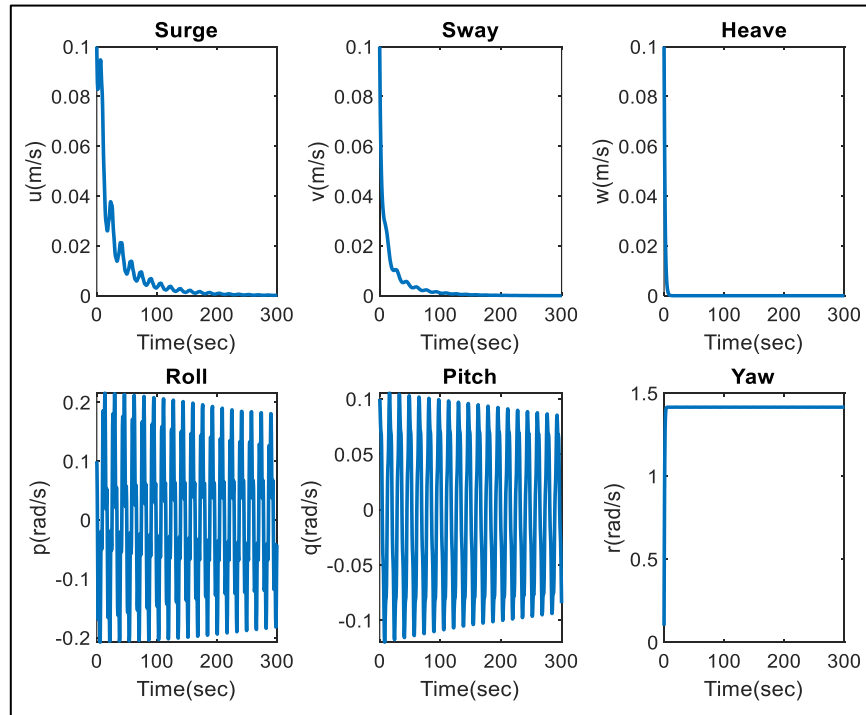
(a)
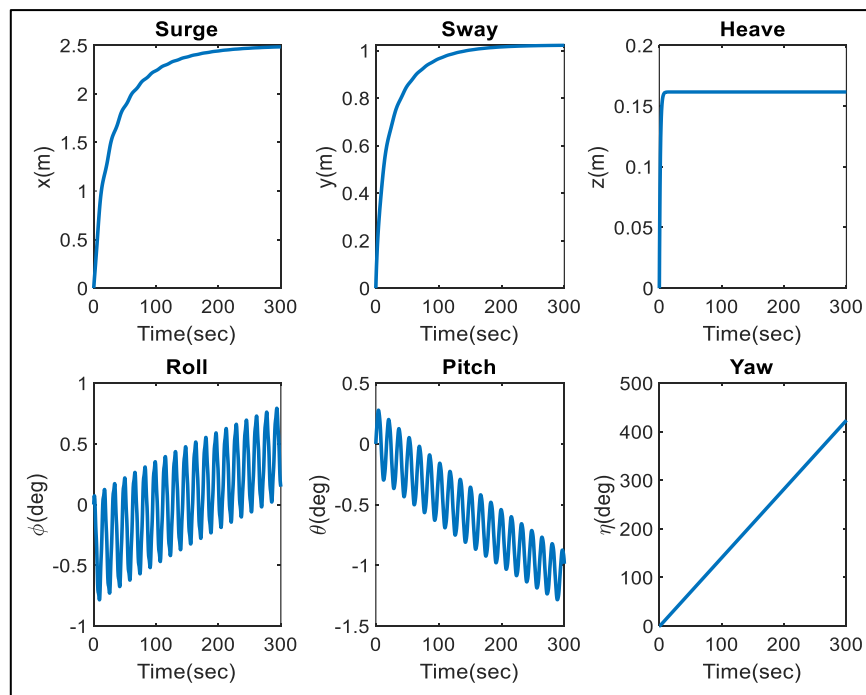
(b)

Figure 9. Performance of ORCA in yaw direction: (a) velocity and (b) position response

ORCA ROV post-fabrication and successive bench tests were deployed in a shallow water region, as shown in Figure 11, to study the behavior of the open loop system (12.931420858589528, 80.22865283652679). Multiple straight-line missions were completed using an open-loop ORCA for a time span of 5-15 mins each along with the IMU connected. The data gathered during these missions were represented graphically as shown in Figures 12 and 13 for comprehensive analysis of the effect of various environmental parameters on the vehicle as well as to study its dynamics as it moves.

The data from IMU was recorded for two successful missions or trials. Mission 1, as shown in Figure 12(a) and (b), focused on forward surge movement where it does show a lot of deviations from the principal direction of movement. This is seen as spikes in the graph. Mission 2, as shown in Figure 13 (a) and (b), also has similar spikes indicating sudden and minor deviation of movement of the vehicle from its principal direction.
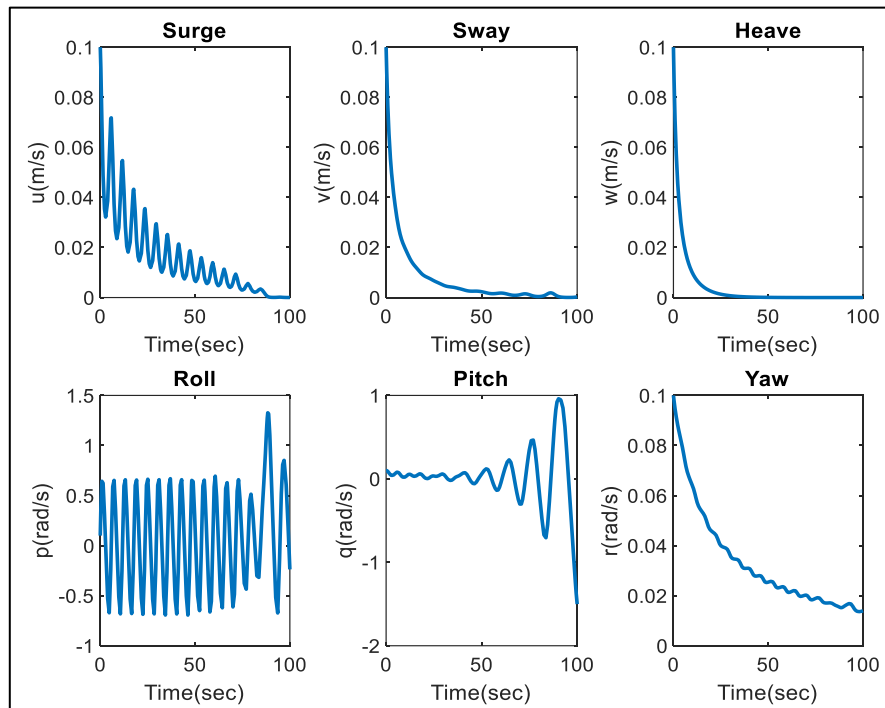
(a)
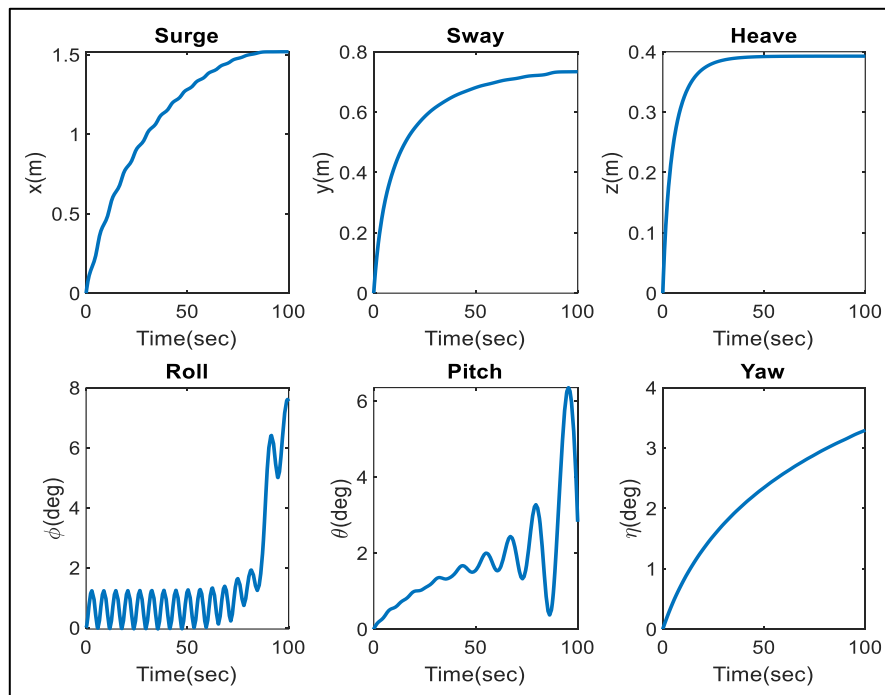
(b)

Figure 10. Performance of ORCA in roll direction: (a) velocity and (b) position response
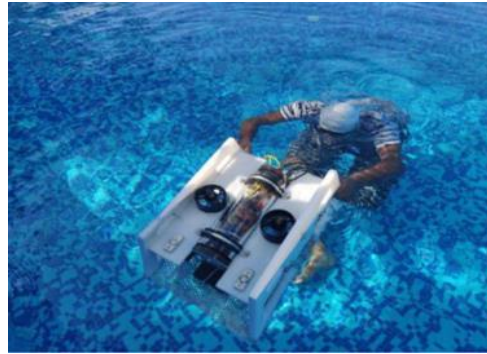
Figure 11. Real time deployment of ORCA

(a)

(b)
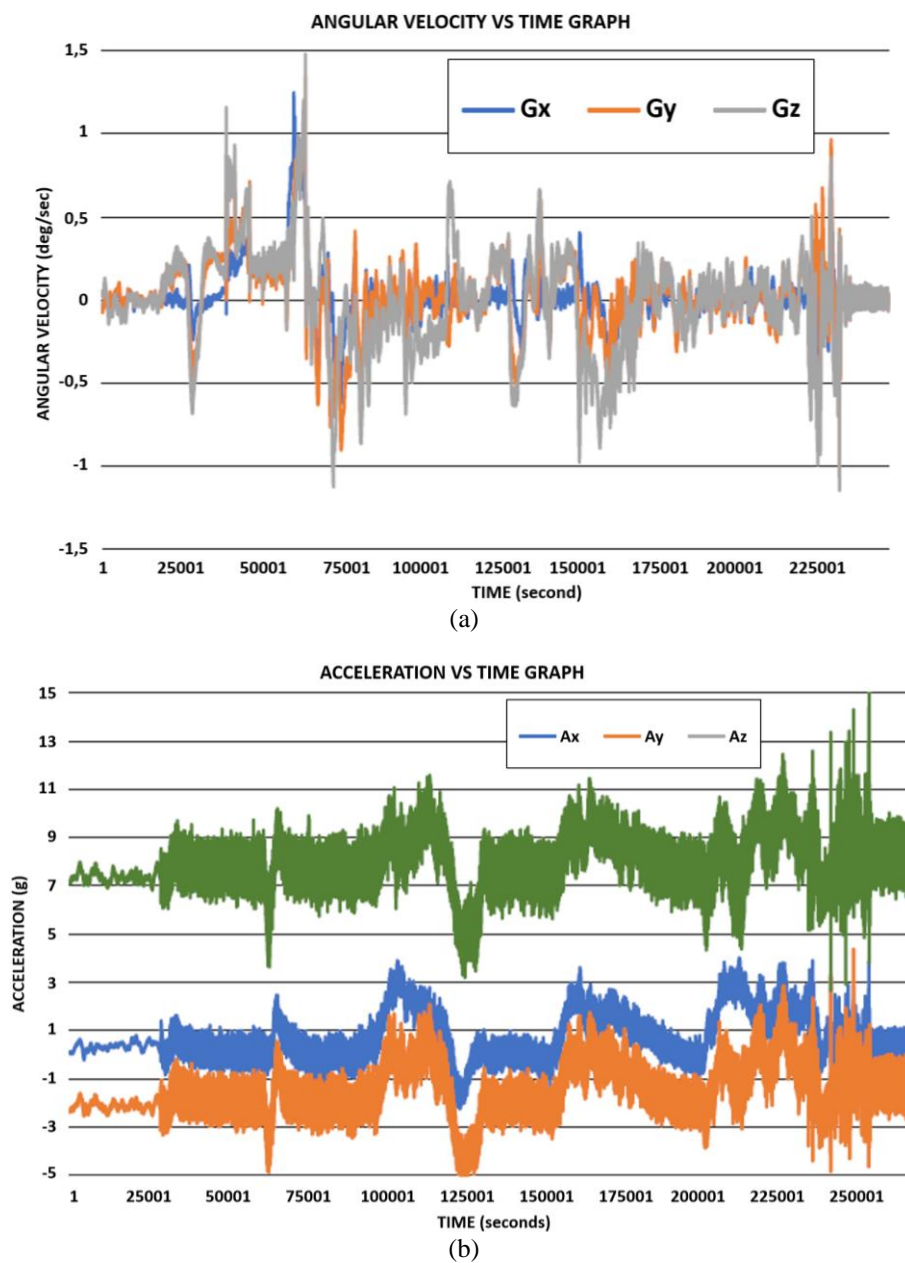
Figure 12. IMU post-processed graphs for (a) the angular velocity versus time and (b) acceleration versus time in mission 1

ACCELERATION VS TIME GRAPH

(a)

ANGULAR VELOCITY VS TIME

(b)
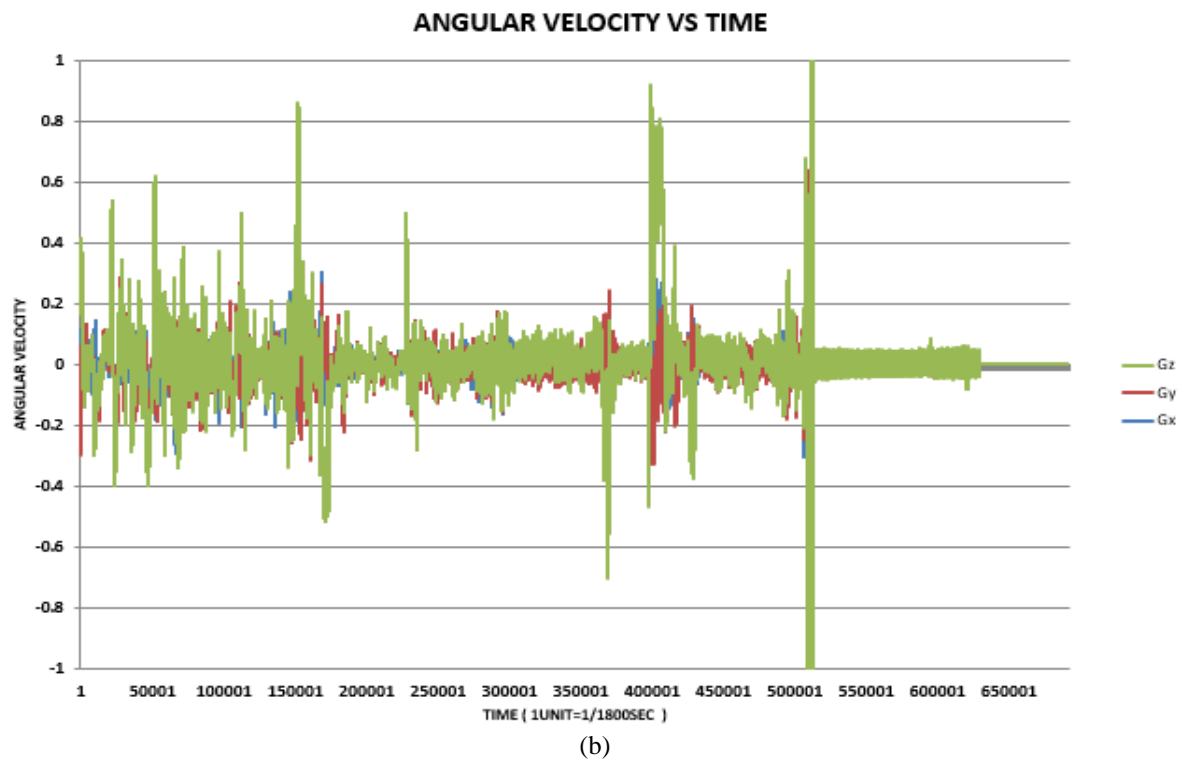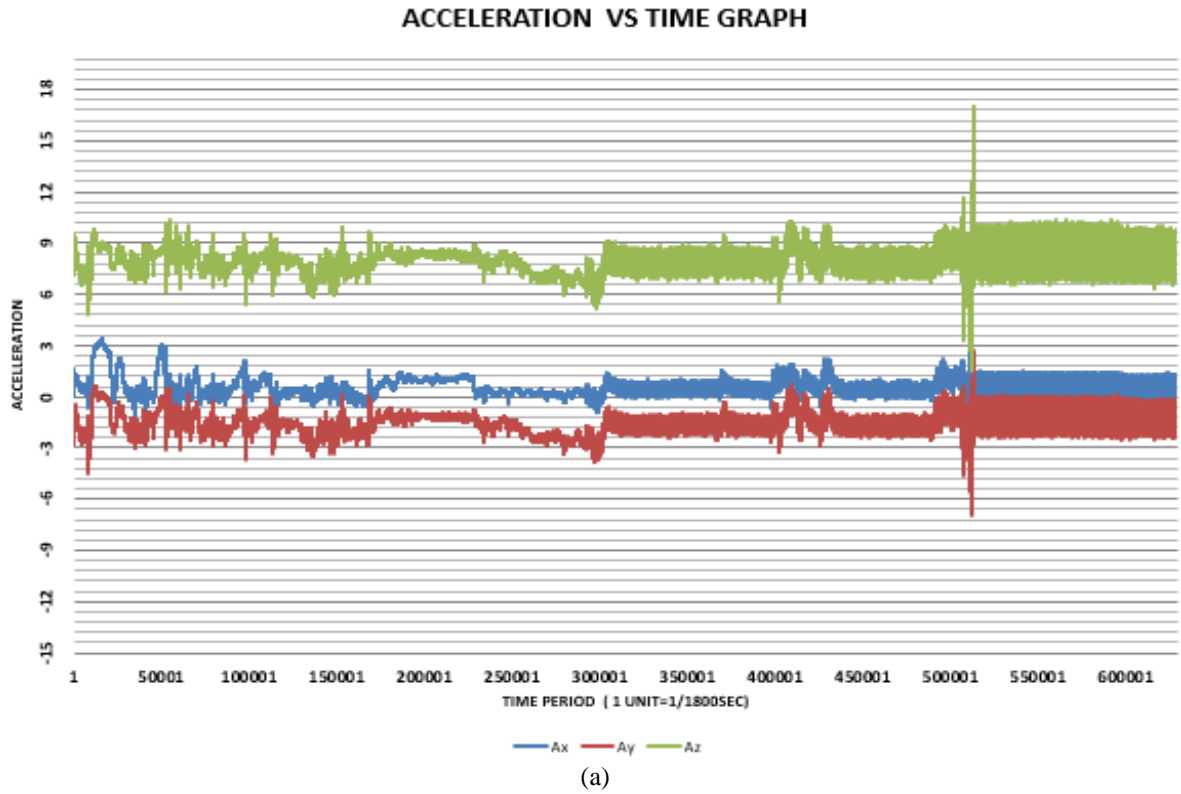
Figure 13. IMU post-processed graphs for (a) acceleration versus time and (b) angular velocity versus time in mission 2

5.   CONCLUSION

This paper aims at discussing the effect of an open-loop controller on the position and velocity responses of ROV-ORCA. The various response graphs suggest that, given 50% thrust to the respective

thrusters to achieve a particular direction of motion, the movement of ROV is not only observed in the principal direction but also in the other directions. Although insignificant, this slight deviation from the path suggests that as the settling time for ROV motion increases, not only does the distance moved from the initial position increase, but also the accumulated error due to the dynamics of the model also increases.

As shown, the open loop ROV induces a significant amount of instability in the other degrees of freedom along with the principal direction of motion. So, the current scope of the work involves analyzing and incorporating various control systems which will enhance the navigation of the vehicle underwater and reduce the error or deviation induced by the external perturbations present underwater. Further, an intense performance analysis is performed on this nonlinear closed-loop ORCA ROV to study its controlled behavior in response to the input command. The control system with a good stability score will be implemented in ORCA which will receive feedback from the inertial measurement unit about its current state and reduce the error to achieve stabilized navigation.

REFERENCES

[1] Y.-H. Lin, S.-Y. Chen, and C.-H. Tsou, "Development of an image processing module for autonomous underwater vehicles through integration of visual recognition with stereoscopic image reconstruction," *Journal of Marine Science and Engineering*, vol. 7, no. 4, p. 107, Apr. 2019, doi: 10.3390/jmse7040107.

[2] J.-K. Choi, T. Yokobiki, and K. Kawaguchi, "ROV-based automated cable-laying system: application to DONET2 installation," *IEEE Journal of Oceanic Engineering*, vol. 43, no. 3, pp. 665–676, Jul. 2018, doi: 10.1109/JOE.2017.2735598.

[3] E. Anderlini, G. G. Parker, and G. Thomas, "Control of a ROV carrying an object," *Ocean Engineering*, vol. 165, pp. 307–318, Oct. 2018, doi: 10.1016/j.oceaneng.2018.07.022.

[4] R. Capocci, E. Omerdic, G. Dooly, and D. Toal, "Fault-tolerant control for ROVs using control reallocation and power isolation," *Journal of Marine Science and Engineering*, vol. 6, no. 2, p. 40, Apr. 2018, doi: 10.3390/jmse6020040.

[5] X. Liu, F. Qi, W. Ye, K. Cheng, J. Guo, and R. Zheng, "Analysis and modeling methodologies for heat exchanges of deep-sea in situ spectroscopy detection system based on ROV," *Sensors*, vol. 18, no. 8, p. 2729, Aug. 2018, doi: 10.3390/s18082729.

[6] S. Sivčev, M. Rossi, J. Coleman, E. Omerdić, G. Dooly, and D. Toal, "Collision detection for underwater ROV manipulator systems," *Sensors*, vol. 18, no. 4, p. 1117, Apr. 2018, doi: 10.3390/s18041117.

[7] R. Capocci, G. Dooly, E. Omerdić, J. Coleman, T. Newe, and D. Toal, "Inspection-class remotely operated vehicles—a review," *Journal of Marine Science and Engineering*, vol. 5, no. 1, p. 13, Mar. 2017, doi: 10.3390/jmse5010013.

[8] D. Khojasteh and R. Kamali, "Design and dynamic study of a ROV with application to oil and gas industries of Persian Gulf," *Ocean Engineering*, vol. 136, pp. 18–30, May 2017, doi: 10.1016/j.oceaneng.2017.03.014.

[9] H.-T. Choi, J. Choi, Y. Lee, Y. S. Moon, and D. H. Kim, "New concepts for smart ROV to increase efficiency and productivity," in *2015 IEEE Underwater Technology (UT)*, Feb. 2015, pp. 1–4. doi: 10.1109/UT.2015.7108257.

[10] O. A. Aguirre-Castro *et al.*, "Design and construction of an ROV for underwater exploration," *Sensors*, vol. 19, no. 24, p. 5387, Dec. 2019, doi: 10.3390/s19245387.

[11] C. Joochim, R. Phadungthin, and S. Srikitsuwan, "Design and development of a remotely operated underwater vehicle," in *2015 16th International Conference on Research and Education in Mechatronics (REM)*, Nov. 2015, pp. 148–153. doi: 10.1109/REM.2015.7380385.

[12] S. Chutia, N. M. Kakoty, and D. Deka, "A review of underwater robotics, navigation, sensing techniques and applications," in *Proceedings of the Advances in Robotics on - AIR '17*, 2017, pp. 1–6. doi: 10.1145/3132446.3134872.

[13] S. K. Nagodagamage, A. M. D. C. Attanayaka, G. S. C. De Silva, and M. S. R. Perera, "AQUABOT: Hydro view real-time video dtreaming remotely operated vehicle," 2015.

[14] G. Conte, S. M. Zanoli, and L. Gambella, "Acoustic mapping and localization of an ROV," in *2006 14th Mediterranean Conference on Control and Automation*, Jun. 2006, pp. 1–6. doi: 10.1109/MED.2006.328873.

[15] G. Karras, D. Panagou, and K. Kyriakopoulos, "Target-referenced localization of an underwater vehicle using a laser-based vision system," in *OCEANS 2006*, Sep. 2006, pp. 1–6. doi: 10.1109/OCEANS.2006.307112.

[16] Y. He, D. B. Wang, and Z. A. Ali, "Measurement and Control," *United Kingdom*. 2020.

[17] "Underwater ROV," *Deep Trekker*. https://www.deeptrekker.com/products/underwater-rov.

[18] C. S. Chin, *Computer-aided control systems design: Practical applications using MATLAB® and Simulink®*. Boca Raton, Florida: CRC Press, 2012.

[19] B. O. A. Haugaløkken, "Motion control systems for ROVs," Norwegian University of Science and Technology, 2014.

[20] L. G. García-Valdovinos, T. Salgado-Jiménez, M. Bandala-Sánchez, L. Nava-Balanzar, R. Hernández-Alvarado, and J. A. Cruz-Ledesma, "Modelling, design and robust control of a remotely operated underwater vehicle," *International Journal of Advanced Robotic Systems*, vol. 11, no. 1, p. 1, Jan. 2014, doi: 10.5772/56810.

[21] C. S. Chin and M. W. S. Lau, *Benchmark models of control system design for remotely operated vehicles*. Singapore: Springer Singapore, 2020. doi: 10.1007/978-981-15-6511-3.

[22] Y. He, D. B. Wang, and Z. A. Ali, "A review of different designs and control models of remotely operated underwater vehicle," *Measurement and Control*, vol. 53, no. 9–10, pp. 1561–1570, Nov. 2020, doi: 10.1177/0020294020952483.

[23]   M. S. Mohd Aras, M. Sulaiman, Y. E. Keong, M. 'Afif Kasno, A. Mohamed Kassim, and A. Khamis, "Performance analysis of
       PID and fuzzy logic controller for unmanned underwater vehicle for depth control," *Journal of Telecommunication, Electronic
       and Computer Engineering (JTEC)*, vol. 9, no. 3–2, pp. 59–63, 2017.

BIOGRAPHIES OF AUTHORS

Tejaswini Panati 🆔 ⑧ SC ⓒ is a graduate student at North Carolina State University, and she is majoring in computer systems networking and telecommunications. She was a part of the undergraduate student team Starboard that developed the ORCA ROV at Sri Sivasubramaniya Nadar College of Engineering. She can be contacted at tejaswini17176@ece.ssn.edu.in.

Sai Deepika I 🆔 ⑧ SC ⓒ is a graduate of electronics and communications from Sri Sivasubramaniya Nadar College of Engineering, Chennai. During her bachelor's, she served as an undergraduate student researcher at the UnderWater Acoustic Research Lab at the Department of ECE and has been a part of the team Starboard that developed the ROV – ORCA. She is interested in the field of communication systems, robotics, sensor integrations, and networking. She can be contacted at sai17138@ece.ssn.edu.in.

Sakthivel Murugan Santhanam 🆔 ⑧ SC ⓒ is an associate professor in the Department of ECE, SSN since June 2001. He obtained his B.E. degree from Madras University and his M.Tech. degree from Pondicherry University. He received his Ph.D. degree from Anna University for his research work on Underwater Signal Processing. His research area of interest is underwater–acoustic communication, signal processing, acoustic wireless sensor networks, green energy harvesting, and deep learning. He established an exclusive research lab for underwater namely Underwater Acoustic Research Lab, in 2014, in the Department of ECE, SSN College of Engineering, which profile can be found at https://sites.google.com/prod/view/uwarlssn. He is a life member of the Indian Society for Technical Education, the Ocean Society of India, and member of Acoustic Society of America. He has acquired projects worth Rs. 109.74 Lakh from various agencies including DST-SSTP, TNSCST, NIOT, and SSN Trust. He can be contacted at sakthivels@ssn.edu.in.